Environ. Sci. Technol. **2007**, *41,* 2756−2763

Measurements of the Volatility of Aerosols from α-Pinene Ozonolysis

CHARLES O. STANIER,*,† RAVI K. PATHAK,‡ AND SPYROS N. PANDIS‡,§

Chemical and Biochemical Engineering Dept., University of Iowa, Iowa City, Iowa 52242, Chemical Engineering Department, Carnegie Mellon University, Pittsburgh, Pennsylvania 15213, and Chemical Engineering Department, University of Patras, Patra 26504, Greece

The temperature-dependence of secondary organic aerosol (SOA) concentrations is measured using a temperature-controlled smog chamber. Aerosols are generated from reaction of α-pinene (14−150 ppb) and ozone at a constant temperature of 22 ± 2°C in the presence of the OH-scavenger 2-butanol. After the reactions are completed the chamber is heated or cooled in a range from 20 to 40 °C. SOA volume concentrations increase at temperatures below the initial formation temperature and decrease at elevated temperatures. The response to the temperature change as measured by percent mass change per degree ranged from −0.4 to −3.6% K^{-1}, for a total mass reduction of 5−60% upon heating from 22 to 35 °C. The reported range is due to two factors: (1) experimental uncertainty, arising mainly from uncertainty in evaporation and condensation behavior of particles lost to the chamber wall; (2) differences in the temperature response from experiment to experiment. Aerosol temperature sensitivity was also measured by tandem differential mobility analysis (TDMA) where similarly generated SOA were heated from 20 to 25 °C to 30−40 °C with residence times of 0.5−1.5 min, resulting in particle volume reductions of up to 20%. The TDMA experiments indicate that evaporation of the SOA particles in this system occurs with a potentially significant mass transfer limitation (e.g., accommodation coefficient <0.1).

1. Introduction

Secondary organic compounds are important constituents of aerosols in urban, rural, and remote areas (*1*−*3*). The potential for secondary organic aerosol (SOA) formation was recognized more than 40 years ago (*4*). Work in environmental chambers in the 1980s showed significant aerosol yields from oxidation reactions of compounds such as α- and β-pinene. With additional chamber experiments, investigators showed that yields depended on aerosol concentration consistent with the formation of an organic solution in the aerosol phase (*5*−*7*). Subsequent studies investigated a variety of related questions of SOA formation and partitioning, including molecular identification of SOA components and the influence of key variables such as temperature, preexisting aerosol, water vapor, heterogeneous reactions, oligomer formation, and scavengers. References on these points can be found in review articles (*8*, *9*).

The goal of this work is to improve understanding of the temperature dependence of SOA concentrations. While there is wide agreement that at least a portion of the secondary organic aerosol is semivolatile and, therefore, should evaporate and condense in response to temperature changes, there is no agreement on the magnitude of the temperature sensitivity of SOA concentrations.

This poorly constrained temperature dependence is an important contributor to uncertainty in chemical transport models (CTMs). CTMs typically use an absorption partitioning model (*5*−*7*) in conjunction with fitted yields from constant temperature smog chamber experiments, and temperature-dependent partitioning coefficients calculated through the Clausius−Clapyeron equation dependent on enthalpies of evaporation (ΔH_{evap}). Values for ΔH_{evap} are taken either from measurements or calculations on compounds that have been isolated in SOA such as pinic acid. Sheehan and Bowman estimated that a 10 °C temperature decrease could increase SOA yields by 20−150% (*10*). Another study showed the potential for a peak in SOA concentrations at 15 °C (*11*); higher temperature caused evaporation while lower temperatures impeded reaction rates. Bian and Bowman showed that surrogate compounds representing a group of compounds need different ΔH_{evap} values than the average of the compounds in the lumped group (*12*). CTM modeling has shown that organic semivolatile partitioning is a leading contributor to SOA concentrations in regional (*13*) and global (*14*) models.

The problem of SOA temperature dependence has been approached in three ways: by TDMA studies, by computational chemistry, and by repeating smog chamber experiments at different temperatures.

Using TDMA, Bilde, and Pandis measured the ΔH_{evap} for solid pinic and trans-norpinic acid particles at 109 and 42 kJ mol^{-1}, respectively (*15*). Bilde and Pandis measured the ΔH_{evap} of glutaric acid at 67 kJ mol^{-1} while 102 was the value reported by Tao and McMurry (*16*). TDMA of complex aerosol is also a well-established experimental technique, although it is typically used at high temperatures (80−300 °C) and short residence times to measure the nonvolatile fraction of particles (*17*−*21*). This volatility TDMA (V-TDMA) has been done for chamber-generated SOA, atmospheric particles, and combustion particles. Neither the single-component TDMA studies nor the V-TDMA experiments solve the problem of SOA temperature dependence because either the chemistry is not atmospherically representative (for single component TDMA) or the temperatures and residences are not (for V-TDMA).

Computational approaches have been widely used, including Kamens (*22*), Kamens and Jaoui (*23*), Cocker et al. (*24*), Capout and Müller (*25*), and Jenkin (*26*). A product distribution (either measured or computed) is used in combination with group contribution methods to establish temperature-dependent vapor pressures or partitioning coefficients. Because of the large number of required assumptions and uncertainties about the chemical makeup of the SOA, the values from these studies can differ appreciably from one another, and to experimental values. Cocker et al. (*24*) found that UNIFAC predicted vapor pressures for the most well-characterized laboratory SOA system (O_3 oxidation of α-pinene under dry conditions), required reduction by a factor of 100 to match experimental yields at 29 °C.

* Corresponding author phone: (319) 335-1399; fax: (319) 335-1415; e-mail: charles-stanier@uiowa.edu.
† University of Iowa.
‡ Carnegie Mellon University.
§ University of Patras.

10.1021/es0519280 CCC: $37.00
Published on Web 03/14/2007

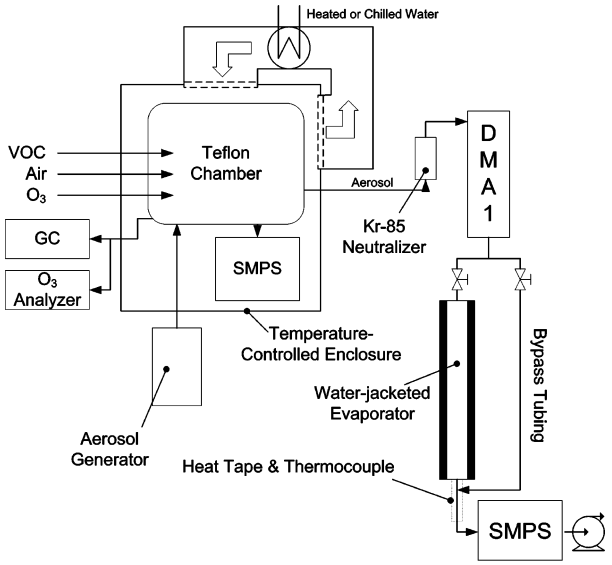

FIGURE 1. Schematic of smog chamber, enclosure and TDMA. Reactions are performed inside the Teflon reactor. Temperature control (for TREVA experiments only; not for TDMA experiments) is provided by a large HVAC system (airflows are depicted by the large open arrows). Gas- and particle-monitoring instruments are deployed inside and around the enclosure.

Repeated chamber experiments at different temperatures have been completed for α-pinene SOA by several investigators (*26*−*29*) and are discussed in a subsequent section. To summarize, the measured temperature sensitivities of the SOA volume vary significantly from study to study (from −0.5 up to −5% K^{-1} for ozonolysis and up to −7% K^{-1} for photooxidation), it is unclear what factors (e.g., chemistry, chamber design, etc.) drive the differences, and adopting the results at the high and low ends of the experimental range would have significant atmospheric implications.

This work presents a direct experimental measurement of the SOA concentration versus temperature relationship at atmospherically relevant temperatures and timescales. A new experimental technique (temperature-ramped volatility analysis, TREVA) is developed. The TREVA experiments are complemented with tandem differential mobility analysis (TDMA) where similar aerosols are exposed to rapid (mass transfer limited) evaporation at atmospherically representative temperatures. For a more extensive discussion of atmospheric implications of SOA temperature dependence, aging, dilution, and representation of these processes, the reader is referred to Donahue et al. (*30*).

2. Experimental Section

The laboratory SOA used in the study was generated by the reaction of α-pinene and ozone inside a Teflon chamber (Figure 1). Two chambers were used: a 5 m^3 chamber for initial experiments, and a 10 m^3 chamber for later experiments (Welch Fluorocarbons, Dover NH). Concentrations of ozone and particles were measured using a continuous ozone analyzer (Dasibi 1008-PC) and a scanning mobility particle sizer (SMPS, TSI 3936), respectively. For some experiments, the α-pinene concentration was monitored by a gas chromatograph (Perkin-Elmer AutoSystem XL with FID and J&W Scientific DB-624 capillary column, 30 m x 0.320 mm). A 3-stage preconcentrator (Entech 7100A, Simi Valley CA) was available for improved VOC quantification.

Reactants included α-pinene in the 14−150 ppb concentration range and ozone produced from an ozone generator (Azco HTU500AC). Reactions were carried out in the presence of an OH-scavenger (2-butanol) in the same concentration ratios (470:1) used by Yu et al. (*31*). Reagents were HPLC or ACS purity grade from Sigma Aldrich. Reactions were carried out under dry conditions (<10% RH) and without a seed aerosol, except for one experiment with ammonium sulfate seed.

Each of the experiments involved a two step process: (1) formation of SOA at 22 ± 2 °C; (2) perturbation of gas-particle partitioning by heating or cooling. The second step was performed by one of two different techniques: (a) temperature-ramped equilibrium volatility analysis (TREVA) heating or cooling of the entire smog chamber and (b) tandem differential mobility analysis, TDMA. TDMA measures the dynamic response of the particles with relatively rapid heating [up to 60 °C/min with a time scale of 0.25−4 min (*15*, *16*, *32*, *33*)]. TREVA (described below) allows the study of temperature changes under longer time-scales at or approaching equilibrium. A list of the experiments is shown in Table 1.

2.1. Variable Temperature Smog Chamber. In the TREVA experiments (Figure 1), the aerosol size distribution was monitored by SMPS as the chamber temperature responded to a step change in the temperature. The SMPS sheath air was recirculated to maintain gas-particle equilibrium during sizing. The SMPS system was located inside the temperature-controlled enclosure so that gas-particle equilibrium was not changed en route to or during particle sizing.

The smog chamber enclosure temperature and DMA temperature (surface mount thermocouple placed on the DMA column) were monitored, and the DMA temperature is used for data reduction in all cases. In experiments with the smaller 5 m^3 Teflon chamber, the difference in these temperatures was typically less than 3 °C and always less than 5 °C, with the DMA temperature lagging the chamber temperature most severely during rapid temperature swings. For experiments with the larger 10 m^3 chamber the maximum temperature difference increased to 8−12 °C for short periods of about 10 min corresponding to the rapid initial heating of the enclosure.

2.2. Tandem Differential Mobility Analysis (TDMA). The TDMA technique (*34*−*36*) uses a heated flow tube to provide a known residence time under conditions favorable to evaporation (elevated temperature and nearly zero gas-phase concentrations of semivolatile species). Shown in Figure 1, the aerosol for evaporation is continuously drawn from the smog chamber through 0.43 cm i.d. copper tubing, traveling to a differential mobility analyzer (DMA1) where a monodisperse aerosol is selected for evaporation. The aerosol travels from DMA1 to DMA2 by one of two possible paths. To measure evaporation, the aerosol travels though a laminar flow evaporator (4 m long, 2.37 cm i.d. stainless tube inside a larger PVC tube with water in the annulus to provide constant temperature). The alternate path is a 0.43 cm i.d. bypass tube at ambient temperature, used to provide a size measurement after minimal (ideally zero) evaporation. The sheath and excess lines of DMA1 are run in a once-through configuration, with sheath air being provided from pressurized air filtered with silica gel, a HEPA filter, and activated carbon. Evaporation begins as the particles encounter the clean sheath air. Additional filtered and preheated dilution air after DMA1 can be introduced to decrease the evaporator residence time. A heating cord and insulation are used to maintain the temperature of the tubing between the evaporator and DMA2 within 1 °C of the air temperature inside the evaporator. Even at the highest flowrates used, centerline temperature came to within 1 °C of wall temperature in the first 0.6 m (out of 4.0 m) of the flow tube. Measurements from previous use of the flow tube showed the average temperature at within 0.1 °C of the wall temperature after 1 m (*37*).

TABLE 1. List of Chamber Experiments

identifier[a]	reactant[b,c]	initial VOC (ppb)	ozone (ppb)	temp. of SOA formation (°C)[d]	subsequent temperature change	volume change[e] (V/V_{init})
TDMA-1	α-pinene	7000	129	22 ± 3	TDMA 20−40 °C	0.83−1.0
TDMA-2	α-pinene	160	320	22 ± 3	TDMA 20−30 °C	0.83−1.0
TDMA-3	α-pinene	100	200	22 ± 3	TDMA 20−40 °C	0.83−1.0
TDMA-4	α-pinene	100	400	22 ± 3	TDMA 20−40 °C	0.80−1.0
TREVA-1	α-pinene	113	600	22 ± 1	*T* increase to 40 °C	0.58, 0.74
TREVA-2	α-pinene	73	400	22 ± 1	*T* increase to 40 °C	0.61, 0.74
TREVA-3	α-pinene	150	600	22 ± 1	*T* increase to 39 °C	0.69, 0.80
TREVA-4	α-pinene	94	400	22 ± 1	*T* increase to 34 °C	0.77, 0.85
					followed by cool to 22 °C	1.13, 1.29
TREVA-5	α-pinene	47	400	22 ± 1	*T* increase to 34 °C	0.80, 0.86
TREVA-6	α-pinene	89	400	22 ± 1	*T* increase to 34 °C	0.71, 0.92
					followed by cool to 24 °C	1.02, 1.24
TREVA-7	α-pinene	14	400	22 ± 1	*T* increase to 34 °C	0.67, 0.86

[a] Experiments TDMA-1 to TREVA-3 were in the 5 m^3 Teflon chamber, while experiments beginning with TREVA-4 were in the 10 m^3 Teflon chamber. [b] All terpene oxidation experiments (with the exception of TDMA-1) were with ozone in excess and 2-butanol as an OH scavenger, based on the protocol of Yu et al. (*41*). [c] All experiments were without seed, except for TREVA-2 which included 900 cm^{-3} ammonium sulfate particles. [d] All experiments were under dry conditions (<10% RH). [e] V_{init} is the volume at the beginning of the temperature change. Reported range for TDMA experiments is due to different residence times and temperatures. Two values in TREVA experiments are from wall loss correction (see eq 1) with $f = 0$ and $f = 1$, respectively.

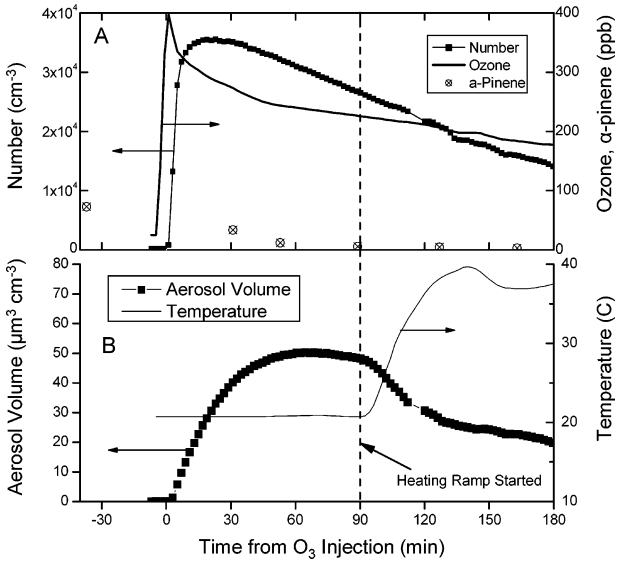

FIGURE 2. Example of raw data from temperature-ramp smog chamber. Panel A shows ozone concentration, aerosol number concentration, and α-pinene concentration. Panel B includes temperature and aerosol volume. Of particular significance to the technique is the fact that, when the temperature is changed at 90 min, the aerosol number continues to decay smoothly while the volume decay increases significantly.

3. Results and Discussion

An example of typical results from a TREVA experiment is shown in Figure 2. 73 ppb α-pinene was initially placed in the smog chamber with the 2-butanol OH-scavenger. Time zero in Figure 2 corresponds to the completion of the ozone injection, which was followed by a rapid increase in the particle number (to 31 000 cm^{-3} in 7 min) and particle mass (to 67 $\mu g\ m^{-3}$ in 50 min) and a drop in α-pinene and ozone concentrations. Aerosol number begins to decline after 20 min, as nucleation of new particles has stopped, and particles are lost to coagulation and the chamber walls. Aerosol volume peaks about 1 h after the ozone injection.

In this experiment, the temperature setpoint of the chamber was changed from 22 to 37 °C at 90 min after the ozone injection. The temperature increase corresponds to a loss of aerosol volume faster than expected from wall losses alone. This can be seen from the changes in slope of the aerosol volume time series at the beginning (94 min) and end (approximately 130 min) of the temperature ramp. No effect can be seen on the aerosol number slope as a result of the temperature ramp.

3.1. TREVA Data Reduction. For quantitative calculation of temperature dependence of aerosol concentrations in the TREVA experiments, we analyze the aerosol mass (C_{oa}) time series. This is calculated assuming spherical particles with densities 1.0, 1.36, and 1.76 for SOA, adipic acid, and ammonium sulfate, respectively, although the final temperature sensitivity is based on concentration ratios and is thus not dependent on the choice of density. This time series is produced after a wall-loss correction (see Appendix for derivation):

$$C_{tot} = C_g + C_{oa}$$

$$C_{oa} = C_{sus} + \frac{C_w S_c}{V_c}$$

$$\frac{d}{dt}\left[\frac{C_w S_c}{V_c}\right] = k_w C_{sus} + f\frac{C_w S_c}{V_c}\frac{1}{C_{sus}}\left[k_w C_{sus} + \frac{d}{dt}C_{sus}\right] \quad (1)$$

where the concentrations C_x are denoted according to subscipts: all semivolatiles in the chamber (C_{tot}); total (wall + suspended) organic aerosol (C_{oa}); gas-phase semivolatiles (C_g); and suspended aerosols (measured by the SMPS, C_{sus}). S_c is the chamber surface area, V_c is the chamber volume, $C_w S_c/V_c$ (units of $\mu g\ m^{-3}$) is the concentration of particles lost to the wall (expressed per volume of chamber), f is an empirical parameter discussed below, and k_w is a first-order loss constant. The use of a size independent wall-loss coefficient is justified because of the monodisperse shape of the secondary organic aerosol size distribution, with log σ_g values of approximately 0.15. To confirm that wall loss rates did not vary too much over the size range of interest, loss coefficients were measured over 11 h at 22 °C with aerosol from α-pinene ozonolysis. First-order loss coefficients (corrected for coagulation) were not size dependent to within experimental uncertainty in the range of interest ($4-7 \times 10^{-5}\ s^{-1}$ at 100 nm and $2-10 \times 10^{-5}\ s^{-1}$ at 200 nm).

Equation 1 is more complicated than typical first-order mass-based wall loss expressions because of the need to account for growth/shrinkage of particles on the chamber wall (by the expression following the parameter *f*). A value of $f = 0$ corresponds to no size change, while $f = 1$ corresponds

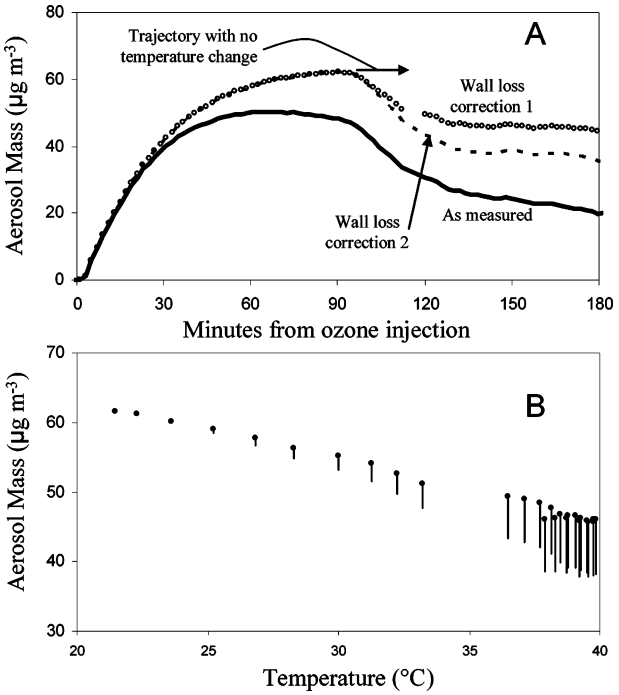

FIGURE 3. Example of wall loss-corrected time series and aerosol temperature response. Panel A graphs temperature together with three values of aerosol mass (as measured, wall loss corrected with $f = 0$ ("wall loss correction 1"), and wall loss correction with $f = 0.5$ ("wall loss correction 2"). Wall loss corrections done with eq 1. Panel B has wall loss corrected aerosol mass graphed versus temperature. Error bars show effect of assumptions regarding evaporation of wall-bound particles. Points calculated from eq 1 with $f = 0$ and bars extending down calculated with $f = 1$.

to wall-bound particles behaving exactly as suspended particles. Given values of f and k_w, $C_w S_c/V_c$ is calculated by numerical integration for each experiment, determining C_{oa}. The parameter k_w is measured for each experiment by a fit of $\ln C_{oa}$ vs t during a period of stable temperature. The parameter f is assumed to be between 0 (lower bound to temperature dependence) and 1.0 (upper bound) and the data is reduced at each limit.

For SOA experiments, the time series of wall-loss corrected aerosol concentration (C_{oa}) is regressed against temperature as $\ln(C_{oa})$ vs T. The slope, which has units of K^{-1} is used as the measure of the aerosol concentration temperature dependence. Values are multiplied by 100 and reported in this work as % K^{-1}.

Figure 3 shows an example of wall-loss corrected time series and aerosol temperature response. Figure 3a graphs three values of aerosol mass (as measured, wall loss corrected with $f = 0$ ("wall-loss correction 1"), and wall loss correction with $f = 1.0$ ("wall-loss correction 2"). Panel B graphs wall loss corrected aerosol mass versus temperature.

The true value of f, and its potential variation between experiments, is not known. While the results in this work are sensitive to the gas-particle partitioning behavior of deposited particles, we note that similar phenomena may be at work in any chamber where the temperature changes over time.

3.2. TREVA Method Evaluation. TREVA was tested with a nonvolatile aerosol (polydisperse ammonium sulfate, number mode 60 nm, initially at 16 000 cm^{-3}). The size distribution was monitored as the enclosure temperature was changed from 24 to 38 °C. The SMPS time series was processed identically to those of the SOA experiments, to extract a temperature sensitivity as the slope of $\ln C$ vs T. The result was $-0.1 \pm 0.3\%$ per K (compared to organic aerosol experiments ranging from -0.4 to -3.6% per K).

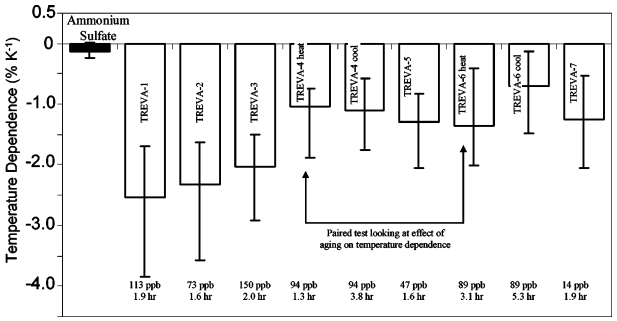

FIGURE 4. Summary plot showing measured volatility for ammonium sulfate and for 9 temperature ramps of α-pinene SOA. Volatility is quantified as % mass change per degree K. Error bars reflect calculated temperature response under two different assumptions regarding the evaporation and condensation of particles on the chamber walls.

The TREVA technique was also challenged with polydisperse adipic acid. TDMA-based experiments from the literature place the saturation concentration of adipic acid at 0.4−0.8 $\mu g\ m^{-3}$ (*16*) and 0.3−1.0 $\mu g\ m^{-3}$ (*38*) at 22 °C, increasing to 3.4−6.7 $\mu g\ m^{-3}$ (*16*) and 4.4−18.2 $\mu g\ m^{-3}$ (*38*) at 36 °C. 74 $\mu g\ m^{-3}$ of adipic acid (C_{tot}) generated using a TSI 3076 atomizer were introduced into the chamber over a 3 h period, followed by a temperature ramp from 20 to 36 °C. At the beginning of the temperature ramp, 18 $\mu g\ m^{-3}$ were suspended while approximately 56 $\mu g\ m^{-3}$ had been lost to the chamber wall and <1 $\mu g\ m^{-3}$ was in the gas phase.

The observed signal was a change in the suspended aerosol concentration (wall-loss corrected) from 18 to 13 $\mu g\ m^{-3}$. Using the aerosol time series with eq 1 and assumed values of f, one can calculate the time history of C_{oa} and C_g (with C_{tot} fixed). Calculating the increase in gas phase adipic acid during the temperature ramp, gives values of 5.4, 22, 36, and 55 $\mu g\ m^{-3}$ for various values of f (0, 0.25, 0.5, and 1, respectively). The difference between the observed change in C_{sus} (5 $\mu g\ m^{-3}$) and the calculated increase in C_g for cases with f > 0, is due to the assumed evaporation of the wall-adhered 56 $\mu g\ m^{-3}$. Based on the expected gas-phase concentration increase of 4−17 $\mu g\ m^{-3}$ from the literature TDMA studies, f should be less than 0.25. However, to be conservative in our reporting of the SOA temperature dependence, rather than generalize this value to the SOA systems, we reduce the SOA data using $f = 0$ and $f = 1$ and report the range.

3.3. TREVA Results for SOA. Applying the data reduction procedure to all the α-pinene experiments gave temperature dependences of aerosol concentration of -0.4 to -3.6% per K. In other words, a one degree temperature increase resulted in a mass or volume loss between 0.4 and 3.6%. The temperature dependences (the slopes of $\ln(C_{oa})$ vs T) are plotted in Figure 4. The wall-loss correction was first performed using $f = 0$. Then, a second calculation was performed with $f = 1.0$. These two values averaged together give the height of the bars in Figure 4.

The uncertainty bounds are calculated by using half of the difference of the individual calculations ($f = 0$ and $f = 1$) and adding the uncertainty from the goodness of fit (2 standard errors on fitted slope). The error bars in the negative direction (i.e., large error bars reflecting potentially greater temperature sensitivity) had an additional term added to account for any upward slope in aerosol concentration at the time of initiation of the temperature ramp. The additional amount was calculated by fitting a second-order polynomial to the 20 min of $C_{oa}(t)$ data prior to the temperature ramp, and extrapolating to determine $C'_{oa}(t_{end})$ where t_{end} is the time of the end of the temperature ramp. The correction is then $[C'_{oa}(t_{end}) - C_{oa}(t_{start})]/[C_{oa}(t_{start})\Delta T]$. This error is

small (up to 0.5% K^{-1}) and scales inversely with the delay between initial SOA formation and the temperature ramp.

The fit of $\ln(C_{oa})$ versus temperature had R^2 values ranging from a low of 0.5 to a high of 0.99. In most cases, the uncertainty in f (0 vs 1) was the larger contributor to uncertainty (in the median case, the choice of f contributed 75% of the uncertainty while the goodness of fit contributed 15% and the upward slope in C_{oa} at the time of the temperature ramp contributed 10%). The error regarding the wall-loss correction and associated choice of the f parameter is likely to be correlated from experiment to experiment, while the uncertainty from the goodness of fit seems to be specific to the individual experiments. The lack of understanding of the evaporation and condensation behavior of particles on the walls, as parametrized by the factor f, is currently the biggest uncertainty in the TREVA technique.

While there is some suggestion that lower concentrations and longer aerosol aging times (all experiments are with ozone in excess) give lower temperature dependences, the error bars in combination with the relatively low number of experiments prevent any definitive conclusion on this point.

3.4. TDMA Results. The TDMA approach and apparatus was tested with polydisperse adipic acid aerosol, which was put in the same 5 m^3 Teflon chamber used for terpene ozonolysis, and then sampled from there into the TDMA system. The aerosol size changes were converted to vapor pressures using the established technique of adjusting the unkown vapor pressure to achieve a match between predicted and observed size changes (*15*, *16*, *36*). The results compared favorably to previously measured values of Tao and McMurry (agreement to ±15%). Using non-evaporating aerosols, the uncertainty on diameter changes was determined to be about ±1%. Absolute accuracy was evaluated with polystyrene latex spheres and was about ±3%.

The TDMA apparatus was used to measure the size change of α-pinene SOA upon heating from 22 °C to temperatures ranging from 30 to 43 °C with mean residence times of up to about 1.5 min. In general, diameter size changes of up to 7% (volume reduction of 20%) were measured, and nearly all experiments were done with initial diameters of 100 or 150 nm. Data is reported in the Supporting Information.

By comparing this evaporation measurement (~7% diameter change at 39−43 °C and residence time of 1 min) with the results for atomized pinic acid (*15*), we immediately see a large difference. For instance, at 39 °C, pinic acid aerosol evaporated almost completely from an initial size of 150 nm in about 20−60 s, corresponding to the measured vapor pressure (at 39 °C) of about $2-8 \times 10^{-9}$ atm (the corresponding c_{sat} is 15−60 $\mu g\ m^{-3}$).

Because of the low amount of measured evaporation in the SOA aerosols relative to pinic acid, various experimental problems that could lead to a low bias in evaporation were examined. The following potential problems were considered: (1) condensation of previously evaporated materials onto aerosols prior to DMA 2 (ruled out by monitoring the TDMA result with different temperatures on the heated transfer line, which had a mean residence time of less than 1 s); (2) evaporation of aerosols in the bypass line used to verify the initial unheated size (ruled out by verifying no systematic difference in the DMA1 setpoint compared to the measured size at DMA2 for ammonium sulfate and unheated secondary organic aerosols); (3) resistance to mass transfer due to non-negligible gas-phase semivolatiles during evaporation (discussed below).

Three causes of non-negligible gas-phase concentrations in the evaporation tube were ruled out: (1) insufficient dilution at DMA1 (ruled out because a 15:1 sheath to aerosol flow ratio was used, and sheath air was carbon filtered to remove organics); (2) build-up of gas-phase concentrations from evaporation of the particles in transit (ruled out by mass balance calculation and keeping number concentrations below 1000 cm^{-3}, thereby ensuring evaporated mass was less than 5% of saturation concentrations); (3) evaporation of previously deposited organics on the evaporation tube wall (ruled out by comparing results with and without overnight heating and flushing of the evaporation tube with 45 °C filtered air.

3.5. Comparison of TDMA and TREVA Results. The TREVA result (at equilibrium) and the TDMA result (under mass transfer limited conditions) are not directly comparable, and therefore, a semivolatile partitioning model is used to enable comparison. Partitioning is described using the absorptive partitioning model (*5*−*7*) as implemented in refs *11*, *39*:

$$Y = \frac{C_{oa}}{\Delta ROG} = C_{oa} \sum \frac{a_i}{c_i^* + C_{oa}} \qquad (2)$$

where Y is the overall aerosol mass yield, C_{oa} is the production of organic aerosol in the chamber ($\mu g\ m^{-3}$), ΔROG is the consumption of reactant ($\mu g\ m^{-3}$), a_i is the stoichiometric yield of semivolatile species i, and c_i^* is the effective saturation concentration of compound i ($\mu g\ m^{-3}$). Changes in the saturation concentration of species i with temperature were described by the Clausius Clapeyron equation:

$$\frac{c_i^*(T_2)}{c_i^*(T_1)} = \frac{T_1}{T_2} \exp\left[\frac{\Delta H_{evap}}{R}\left(\frac{1}{T_1} - \frac{1}{T_2}\right)\right] \qquad (3)$$

where ΔH_{evap} is the enthalpy of evaporation.

Equations 2 and 3 were used in conjunction with mass transfer equations for TDMA to predict aerosol shrinkage in the TDMA tube. The multicomponent TDMA equation is

$$\frac{dm_i}{dt} = \frac{2M_i \pi D_p D_{i,air} x_i p_i^o}{RT} \exp\left[\frac{4\sigma_i M_i}{\rho_i RTD_p}\right] F(Kn_i, \alpha_i) \qquad (4)$$

where x_i is the aerosol mole fraction of species i, M_i is the molar mass of species i, ρ_i is the density, R is the gas constant, T is the temperature, $p_i°$ is the vapor pressure of species i over a flat surface, σ_i is the surface free energy, D_p is the particle diameter, Kn is the Knudsen number, $D_{i,air}$ is the binary diffusivity of species i in air, and α_i are the accommodation coefficients. Equation 4 assumes activity coefficients of unity and zero concentration of the evaporating species in the bulk gas away from the particle. The transition regime correction F(Kn,α) of Fuchs and Sutugin is used (*39*).

To establish the parameters (vapor pressures and mass fractions) for eqs 2 and 4, we performed a regression to find the stoichiometric yields of six surrogate compounds along a "basis set" with 298 K saturation concentrations of 0.01, 0.1, 1, 10, 100, and 1000 $\mu g\ m^{-3}$ (*30*). The data used were the α-pinene ozonolysis SOA yield experiments of Cocker (*24*) together with the TREVA-measured temperature dependences (e.g., Figure 4). More smog chamber experiments can be included in the fitting, but the results are qualitatively the same. Two sets of regression were performed to account for the uncertainty in the temperature dependence as measured by the TREVA technique. The first set, denoted A and B, was performed on the temperature dependences obtained using $f = 0.5$ TREVA data. The second set, denoted C and D, was performed using $f = 0$ values. Different values of ΔH_{evap} were tried in the regression (with the same ΔH_{evap} applied to all the compounds in the basis set), and values of 10−50 kJ mol^{-1} gave the best results. The parameters used for models A through D are listed in Table 2.

TABLE 2. Semivolatile Stoichiometry Used in TREVA Vs TDMA Comparison

model	molar yields binned by compound c_{sat} at 298 K (μg m^{-3})							average absolute error vs (24)	mean bias vs (24)	$\Delta \ln C/\Delta T$ at 30 °C, 10 μg/m^3 (% K^{-1})	$\Delta \ln C/\Delta T$ at 30 °C, 100 μg/m^3 (% K^{-1})
	0.01	0.1	1	10	100	1000	ΔH				
A	0.035	0.030	0	0.057	0.108	0.23	20	0.01	−0.002	−1.10	−1.27
B	0.064	0.051	0	0.025	0.085	0.16	50	0.01	−0.007	−1.06	−1.77
C	0.044	0.029	0	0.071	0.056	0.26	10	0.01	−0.006	−0.70	−0.69
D	0.070	0.062	0	0.043	0.006	0.13	30	0.02	−0.003	−0.60	−0.67

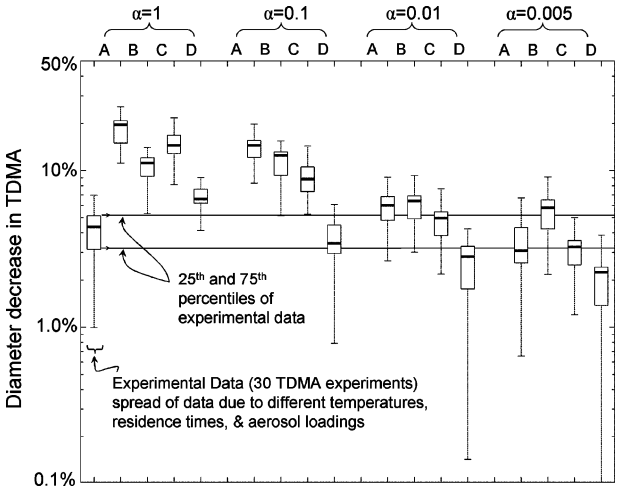

FIGURE 5. TDMA Result. The left-most box is for the experimental data. The rest of the 16 boxes are simulations of particle shrinkage in the TDMA for combinations of accommodation coefficients (1−0.005) and aerosol stoichiometry (A−D). The line inside the box is the median, the box boundaries are at 25th and 75th percentiles, and the whiskers extend to 1.5 interquartile ranges. Models A and B have a mix of semivolatile components with higher temperature dependence because they are fit to the middle of the range of TREVA results. Models C and D are fit to the low-temperature dependence bound of the TREVA results.

Next, TDMA evaporation was simulated using eqs 2−4 (with a value of σ of 0.05 J m^{-2}). These were used to calculate the organic aerosol composition (e.g., mass fractions of semivolatile species) entering the TDMA tube and resulting evaporation for each of the 30 TDMA experiments. This was repeated for different accommodation coefficients, and results are shown in Figure 5. For all cases (A−D) an accommodation coefficient of one would predict more evaporation than observed in the experiments. With 30 experiments, *t*-tests on mean diameter change for the measurements versus models A−D using an accommodation coefficient of one are highly significant, with *p* values of less than 10^{-4}. This assumes 15 and 30% standard errors on the measured and modeled diameter changes. Furthermore, *t* tests are significant to a significance level of 5% even in the presence of bias in the measured or modeled size change of up to ∼0.05 $D_{p,init}$ for cases A−C and up to 0.013 $D_{p,init}$ for case *D*. For models *C* and *D*, accommodation coefficients of ∼0.01 and ∼0.1, respectively, are sufficient to match the range of observed TDMA results. For models A and B, accommodation coefficients below 0.01 are required to sufficiently limit evaporation.

The implication of the TDMA to TREVA comparison, that the accommodation coefficient may be 0.1 or less, has important implications for rapid sampling configurations where adjustment of semivolatile partitioning must be considered, including V-TDMA. We note that while the mass transfer limitation was quantified in terms of accommodation, the exact nature of the kinetic limitation is not understood.

3.6. Comparison to Other Experiments. This work brackets the temperature sensitivity of SOA from α-pinene ozonolysis between −0.4 and −3.6% K^{-1}. This applies to temperatures between about 20 and 37 °C and to ΔROG values between about 14 and 150 ppb (corresponding to C_{oa} concentrations between ∼5 to ∼200 μg m^{-3}). This can be compared to two types of experiments: (1) pure components, and (2) SOA with less than 100 ppb of reacted α-pinene and no organic seed aerosol.

The expected $\Delta \ln C_{oa}/\Delta T$ of a pure compound is easily calculated if *both* the ΔH_{evap} and the aerosol-gas partitioning are known (the formula is $-(1 - x)\Delta H_{evap}/(xRT^2) - 1/T$ where x is the aerosol fraction of the total semivolatiles). Considering a case where ΔH_{evap} is 40 kJ mol^{-1}, the temperature sensitivities are −48, −6, and −0.9% K^{-1} for aerosol fractions of 0.1, 0.5, and 0.9, respectively. For ΔH_{evap} of 110 kJ mol^{-1} and the same aerosol fractions, the temperature sensitivities increase to −130, −15, and −2% K^{-1}.

Turning to experimentally based results, Pathak et al. (*28*) repeated the TREVA experiment in the CMU chamber and obtained a temperature dependence of −1.6% K^{-1} between 15 and 40 °C.

Multiple chamber experiments over a range of temperatures are not directly comparable to TREVA experiments because of the simultaneous influence in the former experiments of temperature on partitioning and gas-phase chemistry (yields of various products, branching ratios in the system of reactions, etc.). Pathak et al. report little to no temperature dependence (0 to −1% K^{-1}) at temperatures above 10 °C using this technique. The results of Sathoff et al. (at 17 ppb α-pinene) are significantly different, with a temperature dependence of about −3% K^{-1} (*29*). Jenkin (*26*) fit experiments from different investigators and different chambers to a detailed model including semivolatile partitioning. At 75 ppb α-pinene oxidized with O_3 in the presence of cyclohexene, the model shows temperature dependence of −4.6% K^{-1}.

Two other works, while not directly comparable, bear mention. Takekawa, with photooxidation of 90 ppb α-pinene (as opposed to ozonolysis with scavenger in this work) reports a large temperature dependence, with the aerosol mass dropping from 89 to 20 μg m^{-3} with the main difference in the experiments being the 10 vs 30 °C temperature (−7.4% K^{-1}). It should be noted that this is from a single pair of experiments. Offenberg et al. (*40*), evaporated SOA from photooxidation, but with major differences in concentrations, chamber configuration, temperatures, residence times, and chemistry.

3.7. Implications for Models. While these discrepancies in the experiments may appear small (e.g., −1 vs −5%), they are significant when applied over a typical atmospheric temperature difference of 15 °C, easily found in a diurnal cycle or between the surface and an elevation of 3 km. For −1% K^{-1} we calculate a small but non-negligible (14%) change in concentration for this 15 °C, while −5% K^{-1} gives a large (53%) change in organic aerosol concentration.

In this work, no ΔH_{evap} values have been reported. The reason for this is that to determine ΔH_{evap} values, the chemical makeup of semivolatiles in the aerosol and gas phases must be quantified (at least the relative amounts of compounds or groups of compounds with distinct saturation concentra-

tions must be known). As a corollary, the expected temperature sensitivity with several semivolatile compounds in solution depends not only on the individual ΔH_{evap} values, but also on the partitioning prior to any temperature modification.

4. Conclusion

This work presents a whole chamber method to look at the temperature sensitivity of SOA concentrations. The uncertainty in the method is due to a lack of understanding of evaporation and condensation of particles on chamber walls. However, TREVA provides a limit (−4% K^{-1}) to the temperature dependence of SOA concentrations from the α-pinene SOA system in the concentration ranges used in this work. The method has the potential to help evaluate kinetic limitations to evaporation of SOA aerosols, and to help decouple temperature-dependent stoichiometry from temperature-dependent partitioning.

Simple SOA parametrizations, when coupled with ΔH_{evap} values as low as 30 kJ mol^{-1}, can exhibit temperature sensitivities inconsistent with these experiments. Potential mass transfer limitations to the evaporation of organic aerosol can be seen in TDMA experiments in the ozone/α-pinene system. Use of both the TDMA and TREVA techniques can help quantify these limitations.

Acknowledgments

We thank Neil Donahue, Tim Raymond, Ray Dagastine, Mirete Bilde, and Kara Huff-Hartz. Although the research described in this manuscript has been funded wholly or in part by the United States Environmental Protection Agency through grant RD-83108101, it has not been subjected to the Agency's required peer and policy review and, therefore, does not necessarily reflect the views of the Agency and no official endorsement should be inferred. Additional funding from NSF-ATM 336296.

Appendix

The equation for the wall loss correction during evaporation-condensation under assumption of size independent first-order wall losses:

$$\frac{d}{dt}[C_{sus}V_c] = -L_w + E_{sus} \quad \text{(A1)}$$

$$\frac{d}{dt}[C_wS_c] = +L_w + E_w \quad \text{(A2)}$$

where C_w is the particle volume concentration on the chamber wall ($\mu g^3\ m^{-2}$), S_c is the chamber surface area (m^2), C_{sus} is the mass concentration of suspended particles inside the chamber ($\mu g^3\ m^{-3}$), and V_c is the chamber volume (m^3). L_w is the mass loss rate of particles to the wall ($\mu g\ min^{-1}$), E_{sus} and E_w are the rate of change of the particle mass in suspension and on the wall, respectively, due to evaporation and condensation ($\mu g\ min^{-1}$). Production of aerosol via reaction is neglected in equations (A1) and (A2) assuming that the analysis is performed after reactions are completed.

Defining an evaporation coefficient β (unit of K^{-1}) where M is aerosol mass and E is an evaporation rate:

$$E = -\frac{dT}{dt}\frac{dM}{dT} = \frac{dT}{dt}\left(\frac{1}{M}\frac{dM}{dT}\right)M = -\frac{dT}{dt}\beta M \quad \text{(A3)}$$

In writing expressions for the evaporation (condensation) rate of suspended and wall-bound particles, we allow the particles on the wall to evaporate at a rate proportional to the suspected particles, with an empirical proportionality constant f.

$$E_{sus} = -\frac{dT}{dt}\beta[C_{sus}V_c] \quad \text{(A4)}$$

$$E_w = -\frac{dT}{dt}f\beta[C_wS_c] \quad \text{(A5)}$$

Substituting these in to equations (A1) and (A2) the equations for rate of change of suspended and wall-associated aerosols are

$$\frac{d}{dt}[C_{sus}V_c] = -L_w + \frac{dT}{dt}\beta[C_{sus}V_c] \quad \text{(A6)}$$

$$\frac{d}{dt}[C_wS_c] = L_w + \frac{dT}{dt}f\beta[C_wS_c] \quad \text{(A7)}$$

Eliminating β gives a differential equation for the concentration of particles on the wall:

$$\frac{d}{dt}[C_wS_c] = L_w + f\frac{C_wS_c}{C_{sus}V_c}\left[L_w + \frac{d}{dt}[C_{sus}V_c]\right] \quad \text{(A8)}$$

When the mass concentration of suspended aerosol is decaying by wall loss alone, the second term is zero, and the wall aerosol increases by exactly L_w.

Writing the L_w term in terms of first-order loss constant k_w and dividing through by the chamber volume V_c gives a differential equation for the unknown term C_wS_c/V_c (units of $\mu g\ m^{-3}$):

$$\frac{d}{dt}\left[\frac{C_wS_c}{V_c}\right] = k_wC_{sus} + f\frac{C_wS_c}{V_c}\frac{1}{C_{sus}}\left[k_wC_{sus} + \frac{d}{dt}C_{sus}\right] \quad \text{(A9)}$$

Supporting Information Available

Experimental results for α-pinene temperature ramp experiments and results of individual TDMA experiments. This material is available free of charge via the Internet at http://pubs.acs.org.

Literature Cited

(1) Turpin, B. J.; Saxena, P.; Andrews, E. Measuring and simulating particulate organics in the atmosphere: problems and prospects. *Atmos. Environ.* **2000**, *34*, 2983−3013.

(2) Andrews, E.; Saxena, P.; Musarra, S.; Hildemann, L. M.; Koutrakis, P.; McMurry, P. H.; Olmez, I.; White, W. H. Concentration and composition of atmospheric aerosols from the 1995 SEAVS experiment and a review of the closure between chemical and gravimetric measurements. *J. Air Waste Manage. Assoc.* **2000**, *50*, 648−664.

(3) Chow, J. C.; Watson, J. G.; Fujita, E. M.; Lu, Z. Q.; Lawson, D. R.; Ashbaugh, L. L. Temporal and spatial variations of pm(2.5) and pm(10) aerosol in the Southern California air-quality study. *Atmos. Environ.* **1994**, *28*, 2061−2080.

(4) Went, F. W. Blue hazes in the atmosphere. *Nature* **1964**, *187*, 641−643.

(5) Pankow, J. F. An absorbtion-model gas-particle partitioning of organic compounds in the atmosphere. *Atmos. Environ.* **1994**, *28*, 185−188.

(6) Pankow, J. F. An absorption-model of the gas aerosol partitioning involved in the formation of secondary organic aerosol. *Atmos. Environ.* **1994**, *28*, 189−193.

(7) Odum, J. R.; Hoffmann, T.; Bowman, F.; Collins, D.; Flagan, R. C.; Seinfeld, J. H. Gas/particle partioning and secondary organic aerosol yields. *Environ. Sci. Technol.* **1996**, *30*, 2580−2585.

(8) Kanakidou, M.; Seinfeld, J. H.; Pandis, S. N.; Barnes, I.; Dentener, F. J.; Facchini, M. C.; Van Dingenen, R.; Ervens, B.; Nenes, A.; Nielsen, C. J.; Swietlicki, E.; Putaud, J. P.; Balkanski, Y.; Fuzzi, S.; Horth, J.; Moortgat, G. K.; Winterhalter, R.; Myhre, C. E. L.; Tsigaridis, K.; Vignati, E.; Stephanou, E. G.; Wilson, J. Organic aerosol and global climate modelling: A review. *Atmos. Chem. Phys.* **2005**, *5*, 1053−1123.

(9) Seinfeld, J. H.; Pankow, J. F. Organic atmospheric particulate material. *Annu. Rev. Phys. Chem.* **2003**, *54*, 121−140.

(10) Sheehan, P. E.; Bowman, F. M. Estimated effects of temperature on secondary organic aerosol concentrations. *Environ. Sci. Technol.* **2001**, *35*, 2129−2135.
(11) Strader, R.; Lurmann, F.; Pandis, S. N. Evaluation of secondary organic aerosol formation in winter. *Atmos. Environ.* **1999**, *33*, 4849−4863.
(12) Bian, F.; Bowman, F. M. Theoretical method for lumping multicomponent secondary organic aerosol mixtures. *Environ. Sci. Technol.* **2002**, *36*, 2491−2497.
(13) Pun, B. K.; Wu, S. Y.; Seigneur, C.; Seinfeld, J. H.; Griffin, R. J.; Pandis, S. N. Uncertainties in modeling secondary organic aerosols: Three-dimensional modeling studies in Nashville/Western Tennessee. *Environ. Sci. Technol.* **2003**, *37*, 3647−3661.
(14) Tsigaridis, K.; Kanakidou, M. Global modelling of secondary organic aerosol in the troposphere: A sensitivity analysis. *Atmos. Chem. Phys.* **2003**, *3*, 1849−1869.
(15) Bilde, M.; Pandis, S. N. Evaporation rates and vapor pressures of individual aerosol species formed in the atmospheric oxidation of alpha- and beta-pinene. *Environ. Sci. Technol.* **2001**, *35*, 3344−3349.
(16) Tao, Y.; McMurry, P. H. Vapor-pressures and surface-free-energies of C14−C18 monocarboxylic acids and C5-dicarboxylic and C6-dicarboxylic acids. *Environ. Sci. Technol.* **1989**, *23*, 1519−1523.
(17) Philippin, S.; Wiedensohler, A.; Stratmann, F. Measurements of non-volatile fractions of pollution aerosols with an eight-tube volatility tandem differential mobility analyzer (VTDMA-8). *J. Aerosol Sci.* **2004**, *35*, 185−203.
(18) Kalberer, M.; Paulsen, D.; Sax, M.; Steinbacher, M.; Dommen, J.; Prevot, A. S. H.; Fisseha, R.; Weingartner, E.; Frankevich, V.; Zenobi, R.; Baltensperger, U. Identification of polymers as major components of atmospheric organic aerosols. *Science* **2004**, *303*, 1659−1662.
(19) Clarke, A. D.; Shinozuka, Y.; Kapustin, V. N.; Howell, S.; Huebert, B.; Doherty, S.; Anderson, T.; Covert, D.; Anderson, J.; Hua, X.; Moore, K. G.; McNaughton, C.; Carmichael, G.; Weber, R. Size distributions and mixtures of dust and black carbon aerosol in Asian outflow: Physiochemistry and optical properties. *J. Geophys. Res.-Atmos.* **2004**, *109*.
(20) Sakurai, H.; Tobias, H. J.; Park, K.; Zarling, D.; Docherty, S.; Kittelson, D. B.; McMurry, P. H.; Ziemann, P. J. On-line measurements of diesel nanoparticle composition and volatility. *Atmos. Environ.* **2003**, *37*, 1199−1210.
(21) Baltensperger, U.; Kalberer, M.; Dommen, J.; Paulsen, D.; Alfarra, M. R.; Coe, H.; Fisseha, R.; Gascho, A.; Gysel, M.; Nyeki, S.; Sax, M.; Steinbacher, M.; Prevot, A. S. H.; Sjoren, S.; Weingartner, E.; Zenobi, R. Secondary organic aerosols from anthropogenic and biogenic precursors. *Faraday Discuss.* **2005**, *130*, 265−278.
(22) Kamens, R. M.; Jang, M.; Chien, C. J.; Leach, K. Aerosol formation from the reaction of α-pinene and ozone using gas-phase kinetics-aerosol partitioning theory. *Environ. Sci. Technol.* **1999**, *35*, 1394−1405.
(23) Kamens, R. M.; Jaoui, M. Modeling aerosol formation from alpha-pinene plus NO_x in the presence of natural sunlight using gas-phase kinetics and gas particle partioning theory. *Environ. Sci. Technol.* **2001**, *35*, 1394−1405.
(24) Cocker, D. R.; Clegg, S. L.; Flagan, R. C.; Seinfeld, J. H. The effect of water on gas-particle partitioning of secondary organic aerosol. Part 1: alpha-pinene/ozone system. *Atmos. Environ.* **2001**, *35*, 6049−6072.
(25) Capouet, M.; Muller, J. F. A group contribution method for estimating the vapour pressures of alpha-pinene oxidation products. *Atmos. Chem. Phys.* **2006**, *6*, 1455−1467.
(26) Jenkin, M. E. Modelling the formation and composition of secondary organic aerosol from alpha- and beta-pinene ozonolysis using MCM v3. *Atmos. Chem. Phys.* **2004**, *4*, 1741−1757.
(27) Takekawa, H.; Minoura, H.; Yamazaki, S. Temperature dependence of aerosol formation by photo-oxidation of hydrocarbons. *Atmos. Environ.* **2003**, *37*, 3413−3424.
(28) Pathak, R. V.; Stanier, C. O.; Donahue, N. M.; Pandis, S. N. Ozonolysis of α-pinene at atmospherically relevant concentrations: Temperature dependence of aerosol mass fractions (yields). *J. Geophys. Res.-Atmos.* **2007**, *112*, D03201, doi: 10.1029/2006JD007436.
(29) Saathoff, H.; Linke, C.; Naumann, K. H.; Wagner, R.; Weingartner, E.; Schurath, U. *Temperature dependence of the yield of secondary organic aerosol from the ozonolysis of α-pinene and limonene*; European Aerosol Conference: Budpest, Hungary, 2004.
(30) Donahue, N. M.; Robinson, A. L.; Stanier, C. O.; Pandis, S. N. Coupled partitioning, dilution, and chemical aging of semivolatile organics. *Environ. Sci. Technol.* **2006**, *40*, 2635−2643.
(31) Yu, F. Q.; Turco, R. P.; Karcher, B. The possible role of organics in the formation and evolution of ultrafine aircraft particles. *J. Geophys. Res.-Atmos.* **1999**, *104*, 4079−4087.
(32) Cruz, C. N.; Dassios, K. G.; Pandis, S. N. The effect of dioctyl phthalate films on the ammonium nitrate aerosol evaporation rate. *Atmos. Environ.* **2000**, *34*, 3897−3905.
(33) Rader, D. J.; McMurry, P. H. The effect of the tandom differential mobility analyzer to studies of droplet growth or evaporation. Application of the tandom differential mobility analyzer to studies of droplet growth or evaporation *J. Aerosol Sci.* **1986**, *17*, 771−787.
(34) Cruz, C. N.; Pandis, S. N. Deliquescence and hygroscopic growth of mixed inorganic-organic atmospheric aerosol. *Environ. Sci. Technol.* **2000**, *34*, 4313−4319.
(35) Rader, D. J.; McMurry, P. H.; Smith, S. Evaporation rates of monodisperse organic aerosols in the 0.02-μm-diameter to 0.2-μm-diameter range. *Aerosol Sci. Technol.* **1987**, *6*, 247−260.
(36) Zhang, S. H.; Seinfeld, J. H.; Flagan, R. C. Determination of particle vapor-pressures using the tandem differential mobility analyzer. *Aerosol Sci. Technol.* **1993**, *19*, 3−14.
(37) Dassios, K. G.; Pandis, S. N. The mass accommodation of ammonium nitrate aerosol. *Atmos. Environ.* **1999**, *33*, 2993−3003.
(38) Bilde, M.; Svenningsson, B.; Monster, J.; Rosenorn, T. Even-odd alternation of evaporation rates and vapor pressures of C3−C9 dicarboxylic acid aerosols. *Environ. Sci. Technol.* **2003**, *37*, 1371−1378.
(39) Seinfeld, J. H.; Pandis, S. N. Atmospheric chemistry and physics: From air pollution to climate change; John Wiley & Sons Inc.: New York, 1998.
(40) Offenberg, J. H.; Kleindienst, T. E.; Jaoui, M.; Lewandowski, M.; Edney, E. O. Thermal properties of secondary organic aerosols. *Geophys. Res. Lett.* **2006**, *33*, L03816, doi:10.1029/2005GL024623.
(41) Yu, J. Z.; Cocker, D. R.; Griffin, R. J.; Flagan, R. C.; Seinfeld, J. H. Gaseous and particulate products. *J. Atmos. Chem.* **1999**, *34*, 207−258.

Received for review September 28, 2005. Revised manuscript received October 13, 2006. Accepted February 6, 2007.

ES0519280